AIP | Applied Physics Letters

Voltage-gated modulation of domain wall creep dynamics in an ultrathin metallic ferromagnet

Uwe Bauer, Satoru Emori, and Geoffrey S. D. Beach

Citation: Appl. Phys. Lett. **101**, 172403 (2012); doi: 10.1063/1.4764071
View online: http://dx.doi.org/10.1063/1.4764071
View Table of Contents: http://apl.aip.org/resource/1/APPLAB/v101/i17
Published by the American Institute of Physics.

Related Articles

Formation of nanoscale magnetic bubbles in ferromagnetic insulating manganite La7/8Sr1/8MnO3
Appl. Phys. Lett. 101, 162401 (2012)

The evolution of magnetic domain structure with magnetic history in amorphous film with perpendicular anisotropy
J. Appl. Phys. 112, 073913 (2012)

Magnetic properties of current-annealed amorphous thin films
J. Appl. Phys. 112, 053910 (2012)

Crossover to striped magnetic domains in Fe1−xGax magnetostrictive thin films
Appl. Phys. Lett. 101, 092404 (2012)

Luminescence-based magnetic imaging with scanning x-ray transmission microscopy
Appl. Phys. Lett. 101, 083114 (2012)

Additional information on Appl. Phys. Lett.

Journal Homepage: http://apl.aip.org/
Journal Information: http://apl.aip.org/about/about_the_journal
Top downloads: http://apl.aip.org/features/most_downloaded
Information for Authors: http://apl.aip.org/authors

ADVERTISEMENT

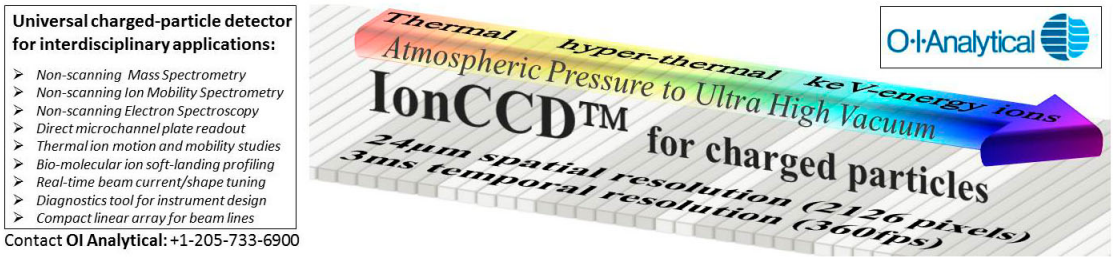

Voltage-gated modulation of domain wall creep dynamics in an ultrathin metallic ferromagnet

Uwe Bauer, Satoru Emori, and Geoffrey S. D. Beach[a)]
Department of Materials Science and Engineering, Massachusetts Institute of Technology, Cambridge, Massachusetts 02139, USA

(Received 13 June 2012; accepted 11 October 2012; published online 24 October 2012)

The influence of gate voltage, temperature, and magnetic field on domain wall (DW) creep dynamics is investigated in Pt/Co/gadolinium oxide (GdOx) films with perpendicular magnetic anisotropy and imaged by a scanning magneto-optical Kerr effect technique. The DW creep velocity can be controlled by an electric field applied to the Co/GdOx interface via a linear modulation of the activation energy barrier with gate voltage. At low speeds, the DW velocity can be changed significantly by a gate voltage, but the effect is diminished as the DW velocity increases, which limits electric field control of fast DW motion. © *2012 American Institute of Physics*. [http://dx.doi.org/10.1063/1.4764071]

Magnetic domain walls (DWs) can encode information for a variety of spintronic memory and logic devices.[1–3] Efficient electrical control of DWs is essential to realizing high-performance solid-state operation of such devices. Much work has focused on using spin-polarized electric currents to manipulate DWs via spin-transfer torque.[4,5] While significantly more efficient than conventional magnetic fields, this mechanism remains dissipative and often suffers from a high critical current for DW displacement. Direct voltage-gated control of DW motion is therefore highly desirable and has been achieved using strain-coupled magnetostrictive/piezoelectric composites,[6–10] but these materials pose challenges to integration with semiconductor processing technology. Recently, it was shown that magnetic anisotropy at the interface between an ultrathin metallic ferromagnet and an oxide dielectric can be modulated by an applied electric field.[11–16] This effect provides a mechanism for direct voltage control of DW propagation in transition metal ferromagnets.[17–19] However, understanding the efficiency and limitations of electric field control of DW dynamics is critical for assessing the potential of voltage-gated DW devices, but this issue has not yet been directly addressed.

In this letter we examine DW dynamics in an ultrathin Co film under the influence of an electric field applied across a gate dielectric. We recently demonstrated that a gate voltage can enhance or retard DW propagation in Pt/Co/gadolinium oxide (GdOx) films, leading to a linear modulation of the propagation field for DW creep motion.[17] Here we present direct space- and time-resolved measurements of DW dynamics spanning more than four decades in velocity using a high-resolution scanning magneto-optical Kerr effect (MOKE) polarimeter. By measuring the velocity scaling with temperature, driving field, and gate voltage, we verify domain expansion via thermally activated creep dynamics and derive an experimentally motivated expression to incorporate magnetoelectric effects into the creep equation of motion. We show that an electric field linearly modulates the activation energy barrier E_a that governs DW creep, and identify consequent limitations to the efficiency of voltage-controlled DW motion. Significant voltage-induced velocity enhancement can be achieved in the low-velocity regime, but the efficiency is diminished at high velocities where E_a is correspondingly small, which limits voltage control of fast DW motion.

Experiments were performed on perpendicularly magnetized Ta(4 nm)/Pt(3 nm)/Co(1 nm)/GdOx(40 nm) films grown at room temperature on thermally oxidized Si(100). Here, the GdOx layer serves as a high-k gate dielectric[20] while simultaneously promoting perpendicular magnetic anisotropy (PMA) in the Co film due to Co-O interfacial hybridization.[21–23] The metal layers were grown by dc magnetron sputtering at 3 mTorr of Ar with background pressure $\sim 1 \times 10^{-7}$ Torr. The GdOx layer was reactively sputtered at an oxygen partial pressure of $\sim 5 \times 10^{-5}$ Torr. After breaking vacuum, 100 μm diameter Ta(1 nm)/Au(5 nm) gate electrodes were deposited through a shadow mask. Magnetic properties were characterized using MOKE and vibrating sample magnetometry (VSM). VSM measurements yielded a saturation magnetization M_s of $\sim$1200 emu/(cm^3 of Co), suggesting minimal Co oxidation during growth of the GdOx overlayer. The films exhibit square out-of-plane hysteresis loops with coercivity $\sim$250 Oe, and in-plane saturation field $\sim$6 kOe, indicating strong PMA.

DW motion was studied using the technique introduced in Ref. 17 and described schematically in Fig. 1(a). A 25 μm diameter blunt W microprobe was used to generate an artificial DW nucleation site through application of a local mechanical stress. After initially saturating the film magnetization, a reversed magnetic field step H was applied using an electromagnet with $\sim$300 μs risetime. The driving field nucleates a reversed domain underneath the W probe tip, which then expands radially across the film. Magnetization reversal was detected via the polar MOKE signal using a $\sim$3 μm diameter focused laser spot positioned by a high-resolution scanning stage. Exemplary time-resolved MOKE transients are shown in Fig. 1(b) for several positions of increasing distance from the W probe tip. Each transient corresponds to the averaged signal acquired from 50 reversal cycles to account for stochasticity and hence represents the integrated probability distribution of

a)Author to whom correspondence should be addressed. Electronic mail: gbeach@mit.edu.

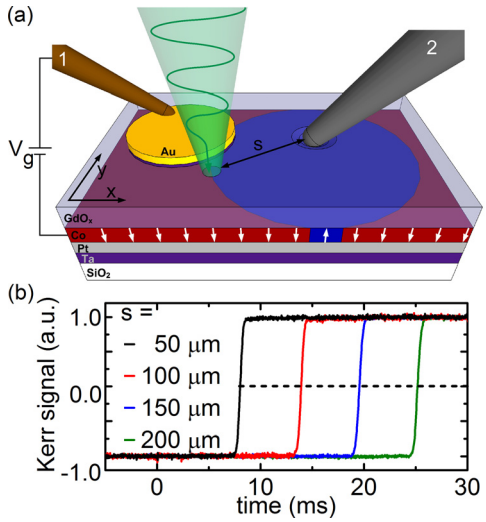

FIG. 1. (a) Experiment schematic showing Pt/Co/GdOx structure. (1) BeCu microprobe for voltage application, (2) W microprobe to create artificial DW nucleation site and focused MOKE laser probe. (b) Normalized MOKE signal transients measured at different distances s between MOKE probing spot and artificial nucleation site.

switching times at a given location.[24] The mean reversal time ($t_{1/2}$), taken as the time at which the probability of magnetization switching is 50%, increases linearly with increasing distance from the nucleation site as expected for DW propagation. The sharp transitions in these averaged transients indicate that DW motion is highly repeatable from cycle to cycle.

By acquiring MOKE signal transients across a two dimensional grid in the vicinity of the nucleation site, the average DW trajectory can be imaged with μm spatial and μs time resolution. Figures 2(a)–2(c) show maps of the normalized polar MOKE signal, corresponding to the perpendicular magnetization component M_z, at several times t after application of a field step $H = 170$ Oe. Figure 2(d) shows a corresponding contour map of the mean reversal time $t_{1/2}$. Here each pixel corresponds to the averaged measurements of 50 reversal cycles. These images show that a reversed domain nucleates beneath the W probe tip and expands radially and isotropically with time. Natural nucleation sites elsewhere in the film are sufficiently distant such that no other DWs reach the probed region under the conditions examined. The remarkably sharp and azimuthally uniform (averaged) DW propagation front suggests smooth DW motion via thermally activated creep through a fine-scale disorder potential. While DW creep is stochastic on the scale of the disorder potential, DW propagation is deterministic at the micrometer-scale resolution of the present experiments.

The dotted circle in Fig. 2(a) outlines the position of a Ta/Au electrode located ~50 μm from the artificial nucleation site. In the absence of a gate voltage, the propagating DW passes unimpeded underneath the electrode. In Figs. 2(e)–2(g) a mechanically compliant 15 μm diameter BeCu probe tip was gently landed on the electrode to apply a gate voltage V_g without creating an additional nucleation site. V_g was limited to ± 8 V to minimize charge trapping and associated irreversibility in the gate oxide.[16,17] Figures 2(e)–2(g) show maps of M_z for $V_g = 8$ V at exactly the same t as the $V_g = 0$ V maps of Figs. 2(a)–2(c). Comparison reveals that at $V_g = 8$ V, domain expansion is impeded underneath the electrode whereas it occurs unimpeded outside of the electrode area. The mean switching time $t_{1/2}$ versus position, plotted in Fig. 2(h), highlights the effect of V_g on DW propagation under the gate electrode. At $V_g = 0$ V, $t_{1/2}$ increases linearly with distance from the nucleation site with the same slope inside and outside the electrode area. However, the slope in the electrode area increases for $V_g = 8$ V and decreases for $V_g = -8$ V, indicating that v increases for $V_g < 0$ and decreases for $V_g > 0$.

To better understand the observed DW dynamics and the role of V_g on those dynamics we measured v as a function of H, V_g, and substrate temperature T. DW velocity was determined from a linear fit of $t_{1/2}$ versus position for typically nine positions across the electrode, on a line extending radially from the artificial nucleation site. In the creep regime of DW dynamics, DW motion is thermally activated and follows an Arrhenius-type relation $v \propto \exp(-E_a(H)/kT)$. Here, k is the Boltzmann constant and E_a the activation energy barrier for DW propagation. E_a is expected to follow a scaling law $E_a \propto (H_{crit}/H)^{\mu}$, where H_{crit} is a characteristic depinning field, and the scaling exponent $\mu = 1/4$ for a one-dimensional elastic line in a two-dimensional disorder potential.[25]

We first measured $v(T)$ at $H = 170$ Oe and $V_g = 0$ V, spanning a temperature range from 25 °C to 55 °C, controlled using a thermoelectric module stable to within ± 0.1 °C. Within this range of T, the velocity spans nearly an order of magnitude. As seen in Fig. 3(a), ln(v) scales linearly with T^{-1}, confirming Arrhenius behavior.[26] The slope corresponds

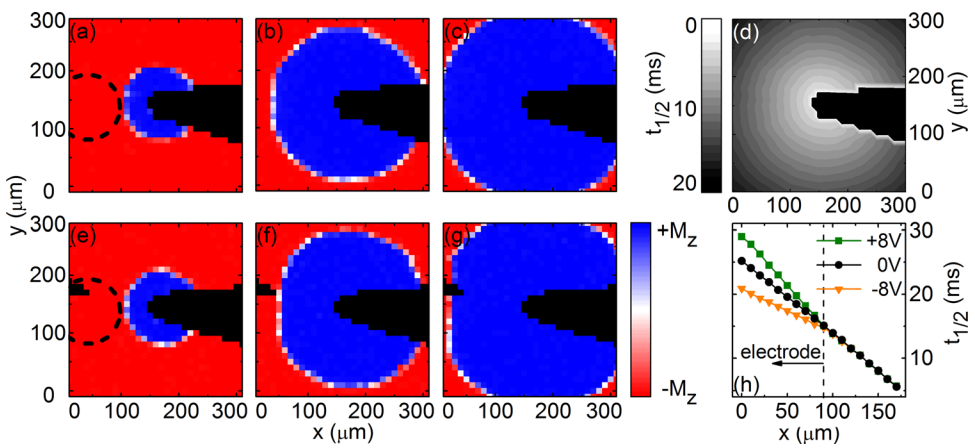

FIG. 2. Polar MOKE maps, showing domain expansion from artificial nucleation site at $t = 6.3$ ms (a), (e), 11.9 ms (b), (f), and 14.7 ms (c), (g) after application of magnetic field step, at $V_g = 0$ V (a)-(c) and at $V_g = 8$ V (e)-(g). (d) Contour map showing mean switching time ($t_{1/2}$) with $V_g = 0$ V. (h) Line scan of $t_{1/2}$ across gate electrode at $V_g = -8$, 0, and +8 V for another device with larger distance between electrode and nucleation site. Black triangular area on right side of (a)-(g) and on left side of (e)-(g) corresponds to W and BeCu microprobe tip, respectively. Dashed black line in (a), (e) outlines gate electrode. All measurements at $H = 170$ Oe and $T = 35$ °C.

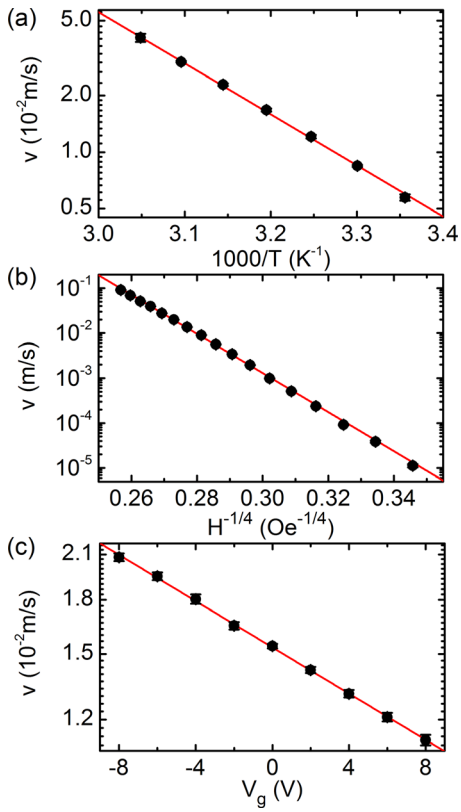

FIG. 3. DW velocity v as a function of (a) temperature (T) at $H = 170$ Oe and $V_g = 0$ V, (b) magnetic field (H) at $T = 35\,^{\circ}$C and $V_g = 0$ V, and (c) gate voltage (V_g) at $H = 170$ Oe and $T = 35\,^{\circ}$C. Red lines are linear fits. Error bars in (a) and (b) are smaller than symbols.

to $E_a = (0.54 \pm 0.01)$ eV, or ~20 kT. In Fig. 3(b), we plot the dependence of v on H over a driving field range from 70 Oe to 230 Oe, corresponding to a change in v by almost four decades. Within this range, the dependence of v on H is well-described via a scaling relation $\ln(v) \propto H^{-1/4}$, consistent with two-dimensional DW creep dynamics.[25]

Having established that DW motion is indeed in the thermally activated creep regime, we proceed to examine the dependence of v on V_g. The depinning field H_{crit} is a function of the DW elastic energy density $\varepsilon_{el} = 4(AK_u)^{1/2}$ and the DW width $\delta = (A/K_u)^{1/2}$, where A is the exchange constant and K_u is the uniaxial anisotropy constant.[25] Therefore, H_{crit} is expected to scale with K_u and voltage-induced changes to K_u are expected to result in a direct modification of E_a and therefore of v. In Fig. 3(c) the dependence of v on V_g is shown at $H = 170$ Oe and $T = 35^{\circ}$C. The DW velocity v can be modified by a factor of two in a bias range of $V_g = -8$ to $+8$ V. Due to limited charge trapping likely at the Co/GdOx interface,[17] we find that the v versus V_g curves often show small hysteresis. Therefore, we plot v averaged over several forward and reverse V_g cycles. Fig. 3(c) shows that $\ln(v)$ and therefore E_a scale approximately linearly with V_g. To accurately access the scaling exponent would require measurements over several decades in v which is experimentally inaccessible. However, in the investigated bias range the scaling relation for v can be expanded to include Vg

$$v(V_g, H, T) \propto \exp\left(-\left(1 + \frac{\alpha}{d_{Ox}} V_g\right) E_{a,0V}(H)/kT\right). \quad (1)$$

Here, d_{Ox} is the GdOx thickness, α is a magnetoelectric coefficient, and $E_{a,0V}$ is the activation energy barrier at $V_g = 0$ V. From the linear fit in Fig. 3(c), the previously determined E_a at $V_g = 0$ V, and taking $d_{Ox} = 40$ nm, we find $\alpha = (8.1 \pm 0.5) \times 10^{-2}$ nm/V.

Given the full functional dependence of v on H, T, and V_g, it is now possible to investigate in more detail the efficiency of voltage control of DW motion across the parameter space. Equation (1) suggests that the relative influence of V_g on v scales with $E_{a,0V}$. The relative DW velocity enhancement, defined here as the ratio between DW velocity at $V_g = -4$ V (v_{-4V}) and at $V_g = 0$ V (v_{0V}) was determined at $T = 35^{\circ}$C for H spanning 100–230 Oe. As H increases, v_{0V} increases exponentially, but the relative enhancement v_{-4V}/v_{0V} decreases (see Fig. 4(a)). At $v_{0V} \approx 2 \times 10^{-4}$ m/s, corresponding to $H = 100$ Oe, we find a voltage-induced velocity enhancement of ~34% at $V_g = -4$ V. However, this same V_g leads to only a ~14% velocity enhancement at $v_{0V} \approx 1 \times 10^{-1}$ m/s, corresponding to $H = 230$ Oe. Therefore, the efficiency of voltage control of DW motion decreases with increasing DW velocity due to the correspondingly lower activation energy barrier.

This behavior follows directly from Eq. (1): an increase in H results in a decrease of $E_{a,0V}$ which then reduces the effect of V_g on the creep velocity. The ratio v_{Vg}/v_{0V} can be expressed as

$$\ln(v_{Vg}/v_{0V}) = -\alpha V_g E_{a,0V}/d_{Ox}kT. \quad (2)$$

Therefore, $\ln(v_{-4V}/v_{0V})$ is expected to decrease linearly with $E_{a,0V}$ at a slope proportional to α. We have determined $E_{a,0V}$ through direct Arrhenius analysis of $\ln(v)$ versus T^{-1} curves, such as shown in Fig. 3(a), at $H = 110$, 130, 150, 170, and 200 Oe. We find that within the measurement accuracy α is independent of H. By plotting v_{-4V}/v_{0V} directly as a function of $E_{a,0V}$ (see Fig. 4(b)) we find that indeed, v_{-4V}/v_{0V} decreases with decreasing $E_{a,0V}$. The linear fit in Fig. 4(b)

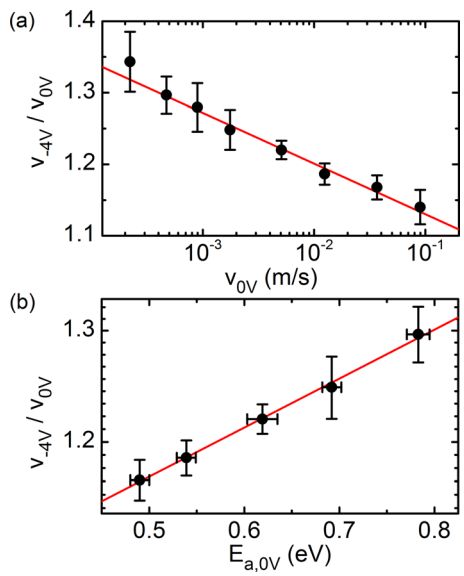

FIG. 4. (a) Ratio between DW velocity at $V_g = -4$ V (v_{-4V}) and at 0 V (v_{0V}) as a function of DW velocity v_{0V}. (b) Subset of same data plotted versus activation energy barrier at $V_g = 0$ V ($E_{a,0V}$). Red lines are linear fits.

yields $\alpha = (9.4 \pm 2.0) \times 10^{-2}$ nm/V, which agrees well with the value determined above.

Taking $E_a \propto K_u$[18,25] and $K_u = K_s/d_{Co} - 2\pi M_s^2$ (with Co film thickness d_{Co} and surface anisotropy constant K_s) this α indicates ~9% electric-field-induced change of E_a at 1 V/nm, corresponding to a ~3% change in K_s. From our VSM results above, we estimate $K_s \approx 1.3$ erg/cm^2 and an electric-field-induced modification of $\sim 3 \times 10^{-9}$ erg/V cm (~30 fJ/Vm).

Large voltage-induced velocity enhancements up to a factor of 10 were recently reported in Refs. 18 and 19, which might enhance the speed of DW-based devices and decrease power consumption.[18,19] However, Eq. (2) and Fig. 4 show that this enhancement depends strongly on the velocity regime probed, and efficiency is diminished as v increases. Reference 18 suggested that velocity enhancement by a factor of 10^5 could be reasonably expected through materials engineering. Based on the α reported here, even at $V_g = -40$ V, corresponding to an electric field of 1 V/nm (typical breakdown limit for high-quality dielectrics), Eq. (2) would require $E_{a,0V} \sim 3$ eV to achieve this enhancement. Extrapolating from Fig. 4(a), this would correspond to toggling the velocity from between $\sim 10^{-18}$ m/s and 10^{-13} m/s, timescales that are experimentally inaccessible and of questionable utility to device operation. A further increase of α by an order of magnitude would be necessary to access practical DW velocities.

In summary, we demonstrate voltage control of DW creep dynamics in Pt/Co/GdOx films and characterize the efficiency of the effect. DW velocity can be controlled by a linear modulation of the activation energy barrier via voltage-induced changes to the interfacial anisotropy. At low DW speeds corresponding to a large activation energy barrier, DW velocity can be significantly modified by a gate voltage. However, at higher speeds the efficiency of voltage control is diminished due to the simultaneous decrease in activation energy, which limits the utility of the effect in high-speed DW-based device applications.

This work was supported under NSF-ECCS-1128439. S.E. acknowledges financial support by the NSF Graduate Research Fellowship Program. Technical support from David Bono and Mike Tarkanian is gratefully acknowledged.

[1]C. Chappert, A. Fert, and F. N. Van Dau, Nat. Mater. **6**, 813 (2007).
[2]D. A. Allwood, G. Xiong, C. C. Faulkner, D. Atkinson, D. Petit, and R. P. Cowburn, Science **309**, 1688 (2005).
[3]S. S. P. Parkin, M. Hayashi, and L. Thomas, Science **320**, 190 (2008).
[4]G. S. D. Beach, M. Tsoi, and J. L. Erskine, J. Magn. Magn. Mater. **320**, 1272 (2008).
[5]A. Brataas, A. D. Kent, and H. Ohno, Nat. Mater. **11**, 372 (2012).
[6]T. K. Chung, G. P. Carman, and K. P. Mohanchandra, Appl. Phys. Lett. **92**, 112509 (2008).
[7]T. H. E. Lahtinen, J. O. Tuomi, and S. van Dijken, Adv. Mater. **23**, 3187 (2011).
[8]J. Dean, M. T. Bryan, T. Schrefl, and D. A. Allwood, J. Appl. Phys. **109**, 023915 (2011).
[9]T. H. E. Lahtinen, K. J. A. Franke, and S. van Dijken, Sci. Rep. **2**, 258 (2012).
[10]N. Lei, T. Devolder, G. Agnus, P. Aubert, L. Daniel, J. V. Kim, W. Zhao, C. Chappert, D. Ravelosona, and P. Lecoeur, e-print arXiv:1201.4939.
[11]M. Weisheit, S. Fahler, A. Marty, Y. Souche, C. Poinsignon, and D. Givord, Science **315**, 349 (2007).
[12]T. Maruyama, Y. Shiota, T. Nozaki, K. Ohta, N. Toda, M. Mizuguchi, A. A. Tulapurkar, T. Shinjo, M. Shiraishi, S. Mizukami, Y. Ando, and Y. Suzuki, Nat. Nanotechnol. **4**, 158 (2009).
[13]M. Endo, S. Kanai, S. Ikeda, F. Matsukura, and H. Ohno, Appl. Phys. Lett. **96**, 212503 (2010).
[14]W.-G. Wang, M. Li, S. Hageman, and C. L. Chien, Nat. Mater. **11**, 64 (2012).
[15]Y. Shiota, T. Nozaki, F. Bonell, S. Murakami, T. Shinjo, and Y. Suzuki, Nat. Mater. **11**, 39 (2012).
[16]U. Bauer, M. Przybylski, J. Kirschner, and G. S. D. Beach, Nano Lett. **12**, 1437 (2012).
[17]U. Bauer, S. Emori, and G. S. D. Beach, Appl. Phys. Lett. **100**, 192408 (2012).
[18]A. J. Schellekens, A. van den Brink, J. H. Franken, H. J. M. Swagten, and B. Koopmans, Nat. Commun. **3**, 847 (2012).
[19]D. Chiba, M. Kawaguchi, S. Fukami, N. Ishiwata, K. Shimamura, K. Kobayashi, and T. Ono, Nat. Commun. **3**, 888 (2012).
[20]T. M. Pan, C. S. Liao, H. H. Hsu, C. L. Chen, J. D. Lee, K. T. Wang, and J. C. Wang, Appl. Phys. Lett. **87**, 262908 (2005).
[21]A. Manchon, S. Pizzini, J. Vogel, V. Uhlir, L. Lombard, C. Ducruet, S. Auffret, B. Rodmacq, B. Dieny, M. Hochstrasser, and G. Panaccione, J. Appl. Phys. **103**, 07A912 (2008).
[22]B. Rodmacq, A. Manchon, C. Ducruet, S. Auffret, and B. Dieny, Phys. Rev. B **79**, 024423 (2009).
[23]M. K. Niranjan, C. G. Duan, S. S. Jaswal, and E. Y. Tsymbal, Appl. Phys. Lett. **96**, 222504 (2010).
[24]S. Emori, D. C. Bono, and G. S. D. Beach, J. Appl. Phys. **111**, 07D304 (2012).
[25]S. Lemerle, J. Ferre, C. Chappert, V. Mathet, T. Giamarchi, and P. Le Doussal, Phys. Rev. Lett. **80**, 849 (1998).
[26]S. Emori and G. S. D. Beach, J. Phys.: Condens. Matter **24**, 024214 (2012).